BIT manuscript No.
(will be inserted by the editor)

Convex source support in three dimensions

Martin Hanke · **Lauri Harhanen** · **Nuutti Hyvönen** · **Eva Schweickert**

Received: date / Accepted: date

Abstract This work extends the algorithm for computing the convex source support in the framework of the Poisson equation to a bounded three-dimensional domain. The convex source support is, in essence, the smallest (nonempty) convex set that supports a source that produces the measured (nontrivial) data on the boundary of the object. In particular, it belongs to the convex hull of the support of any source that is compatible with the measurements. The original algorithm for reconstructing the convex source support is inherently two-dimensional as it utilizes Möbius transformations. However, replacing the Möbius transformations by inversions with respect to suitable spheres and introducing the corresponding Kelvin transforms, the basic ideas of the algorithm carry over to three spatial dimensions. The performance of the resulting numerical algorithm is analyzed both for the inverse source problem and for electrical impedance tomography with a single pair of boundary current and potential as the measurement data.

The work of L. Harhanen and N. Hyvönen was supported by the Finnish Graduate School in Computational Sciences FICS, the Finnish Funding Agency for Technology and Innovation TEKES (contract 40370/08) and the Academy of Finland (the Centre of Excellence in Inverse Problems Research and projects 115013 and 135979).

M. Hanke
Institut für Mathematik, Johannes Gutenberg-Universität Mainz, 55099 Mainz, Germany.
E-mail: hanke@math.uni-mainz.de

L. Harhanen
Department of Mathematics and Systems Analysis, Aalto University, P.O. Box 11100, FI-00076 Aalto, Finland.
E-mail: lauri.harhanen@tkk.fi

N. Hyvönen
Department of Mathematics and Systems Analysis, Aalto University, P.O. Box 11100, FI-00076 Aalto, Finland.
E-mail: nuutti.hyvonen@hut.fi

E. Schweickert
Institut für Mathematik, Johannes Gutenberg-Universität Mainz, 55099 Mainz, Germany.
E-mail: eva.schweickert@gmx.de

Keywords Electrical impedance tomography · convex source support · obstacle problem · inverse elliptic boundary value problem

Mathematics Subject Classification (2000) 65N21 · 35R30

1 Introduction

We consider the inverse source problem for the Laplacian in an insulated, bounded domain $D \subset \mathbb{R}^3$. More precisely, our goal is to introduce a noniterative numerical algorithm for extracting information about the mean-free, compactly supported (distributional) source F in the Poisson equation

$$\Delta u = F \quad \text{in } D, \qquad \frac{\partial u}{\partial \nu} = 0 \quad \text{on } \partial D, \qquad \int_{\partial D} u \,\mathrm{d}s = 0 \tag{1.1}$$

from the value of the potential u on the boundary ∂D. Source problems of this kind are encountered, e.g., in *electroencephalography* (EEG) and geophysics; see [13,19] and the references therein.

It is easy to see that there exists an infinite number of sources that produce the same boundary potential on ∂D (cf., e.g., [8,19]). This issue of nonuniqueness is often circumvented by assuming some specific form for the admissible sources, e.g., Dirac deltas, dipoles, or characteristic functions; see [8,9,10,19,20,21,30]. In [22], Kusiak and Sylvester introduced an alternative approach in the framework of inverse scattering by introducing the *convex scattering support*, which they defined as the intersection of the convex hulls of the supports of all sources that are compatible with a given far field pattern of a scattered wave. The convex scattering support has many useful properties: It is, in essence, the smallest convex set that carries a source that is compatible with the measured data, it is nonempty for nontrivial measurements and, remarkably, it can be defined in a constructive manner that enables numerical implementation. Generalizations of the convex scattering support formalism have since been studied in several articles: for inverse scattering and the Helmholtz equation in [4,11,23,25,27,28] and for electrostatics and *electrical impedance tomography* (EIT) in [12,15,16,17,18], where the term *convex source support* (CSS) is used instead of convex scattering support.

Although the background theory for the CSS is independent of the spatial dimension, the corresponding algorithm, introduced in [16], is inherently two-dimensional as it utilizes tools of complex analysis — most notably, Möbius transformations. The purpose of this work is to demonstrate that the CSS reconstruction technique can, in fact, be carried over to three dimensions by replacing the said Möbius transformations by Kelvin transforms corresponding to inversions with respect to suitable spheres; take note that some of the related analysis was presented already in [26]. Since the interplay between Kelvin transforms and the homogeneous Neumann boundary condition of (1.1) is nontrivial, the resulting numerical algorithm is slightly more complicated than its counterpart in two dimensions. Be that as it may, our numerical experiments show that the three-dimensional version still provides information on the location and the size of the target source without any prior knowledge about its physical properties. Moreover, we also demonstrate that our algorithm can localize inhomogeneities using a single relative boundary potential of EIT as the input data; for more details about EIT, we refer to the review articles [3, 6, 29].

This text is organized as follows. In Section 2, we recall the definition and the basic properties of the CSS. Section 3 describes a constructive way of defining the CSS in three spatial dimensions; in particular, the needed inversions and Kelvin transforms are defined there. The numerical algorithm is introduced in Section 4 and its functionality is tested with simulated data in Section 5. Finally, Section 6 lists the concluding remarks.

2 Convex source support

In this section, we recall the definition and properties of the CSS; for a more complete review of the results needed in the subsequent sections we refer to [16, Section 2]. Assume that $D \subset \mathbb{R}^3$ is a bounded, simply connected domain with a smooth enough boundary. As noted in [15], the problem (1.1) has a well defined, unique solution $u \in \cup_{m\in\mathbb{Z}} H^m(D)$ for any distributional source F in

$$\mathscr{E}'_\diamond(D) = \left\{ v \in \mathscr{E}'(D) \mid \langle v, 1\rangle = 0 \right\},$$

where $\langle \cdot,\cdot\rangle : \mathscr{E}'(D) \times \mathscr{E}(D) \to \mathbb{C}$ denotes the dual evaluation between compactly supported distributions and smooth functions in D. (To be precise, [15, 16] consider only the two-dimensional case, but the spatial dimension plays no role in the considerations of this section.) Moreover, the potential u is smooth in some neighborhood of the boundary ∂D, and thus the linear operator

$$L : F \mapsto u|_{\partial D}, \qquad \mathscr{E}'_\diamond(D) \to L^2_\diamond(\partial D)$$

is well defined. Here, $L^2_\diamond(\partial D)$ denotes the space of square integrable mean-free functions on ∂D.

It is easy to see that L is not injective and not even the support of F is uniquely determined by the boundary measurement $g = LF$ (cf. [15, 22]). What is more, the intersection of the supports of the sources compatible with g is in general empty (cf. [22]), and this may hold even if the holes in the supports are included before the intersection [15]. However, intersecting the convex hulls of the supports of the compatible sources does provide information on the original source as explained in the following (cf. [15, 16]).

The *convex support* $\mathrm{supp}_c F$ of $F \in \mathscr{E}'_\diamond(D)$ is the convex hull of the support $\mathrm{supp}\, F$ of F. Furthermore, the *convex source support* $\mathscr{C} g$ is given by

$$\mathscr{C} g = \bigcap_{LF=g} \mathrm{supp}_c F \tag{2.1}$$

if $g \in \mathscr{R}(L)$, and $\mathscr{C} g$ is defined to be the convex hull $\mathrm{ch}\, D$ otherwise. It can be shown that $\mathscr{C} g$ is essentially the smallest convex set that carries a source that is compatible with g; the following theorem is a restatement of [16, Theorem 2.1]. Here and in the following, $N_\varepsilon(\Omega)$ denotes the open ε-neighborhood of a set $\Omega \subset \mathbb{R}^3$.

Theorem 2.1 *Let $g \in \mathscr{R}(L)$. Then, given any $\varepsilon > 0$, there exists a source $F_\varepsilon \in \mathscr{E}'_\diamond(D)$ such that $LF_\varepsilon = g$ and*

$$\mathscr{C}g \subset \operatorname{supp}_c F_\varepsilon \subset \overline{N_\varepsilon(\mathscr{C}g)}.$$

Moreover, $\mathscr{C}g = \emptyset$ if and only if $g = 0$.

2.1 Extension to a ball

In the following sections we describe our detection algorithm for the case where the domain of interest is a ball. To motivate this choice, let us consider how the knowledge of the measurement g on ∂D, corresponding to a source contained in D, enables a stable way of constructing the measurement corresponding to the same source and an origin-centered ball $B_\rho \supset \overline{D}$ of large enough radius $\rho > 0$. At the same time, we will explain how the convex source support is affected by such an extension process.

Let us consider the transmission problem

$$\begin{aligned} &\Delta w = 0 \quad \text{in } B_\rho \setminus \partial D, \qquad \frac{\partial w}{\partial \nu} = 0 \quad \text{on } \partial B_\rho, \qquad \int_{\partial B_\rho} w \,\mathrm{d}s = 0, \\ &\frac{\partial w^+}{\partial \nu} - \frac{\partial w^-}{\partial \nu} = 0, \qquad w^+ - w^- = g \quad \text{on } \partial D, \end{aligned} \tag{2.2}$$

where $g = u|_{\partial D}$ for the solution of (1.1) and the superscripts $+$ and $-$ denote traces taken from within $B_\rho \setminus \overline{D}$ and D, respectively. The problem (2.2) has a unique solution $w_\rho \in H^1(D) \oplus H^1(B_\rho \setminus \overline{D})$, which can be presented, e.g., in the form of a double layer potential. We denote the zero continuation of u to the whole of B_ρ by u_0 and set $u_\rho = u_0 + w_\rho$. According to [16, Lemma 2.2], this $u_\rho \in \cup_{m\in\mathbb{Z}} H^m(B_\rho)$ is the unique solution of the Poisson problem

$$\Delta u = F \quad \text{in } B_\rho, \qquad \frac{\partial u}{\partial \nu} = 0 \quad \text{on } \partial B_\rho, \qquad \int_{\partial B_\rho} u \,\mathrm{d}s = 0. \tag{2.3}$$

Hence, given the boundary potential $g \in L^2_\diamond(\partial D)$ corresponding to (1.1) with a source $F \in \mathscr{E}'_\diamond(D) \subset \mathscr{E}'_\diamond(B_\rho)$, solving (2.2) provides a stable way to compute the 'propagated' data $g^\rho \in L^2_\diamond(\partial B_\rho)$ corresponding to (2.3) and the very same source.

Let L_ρ be the operator that maps a source $F \in \mathscr{E}'_\diamond(B_\rho)$ onto the Dirichlet boundary value of the solution to (2.3) on ∂B_ρ. The convex source support of $g^\rho \in L^2_\diamond(\partial B_\rho)$ is defined in accordance with (2.1), i.e.,

$$\mathscr{C}_\rho g^\rho = \bigcap_{L_\rho F = g^\rho} \operatorname{supp}_c F \tag{2.4}$$

if $g^\rho \in \mathscr{R}(L_\rho)$, and $\mathscr{C}_\rho g^\rho = B_\rho$ otherwise. The following theorem, which relates $\mathscr{C}g$ and $\mathscr{C}_\rho g^\rho$, is a simplified version of [16, Theorem 2.3].

Theorem 2.2 *If $g = LF$ and $g^\rho = L_\rho F$ for some $F \in \mathscr{E}'_\diamond(D) \subset \mathscr{E}'_\diamond(B_\rho)$, then $\mathscr{C}_\rho g^\rho \subseteq \mathscr{C}g$, where equality holds if D is convex.*

Notice that in general the sets $\mathscr{C}g$ and $\mathscr{C}_\rho g^\rho$ of Theorem 2.2 do not coincide if D is nonconvex [16, Example 1]. To sum up, if D is convex, the convex source support is not affected by extending the source problem to a ball containing the original domain D. If D is nonconvex, this procedure can make the convex source support smaller. However, in any case the new convex source support is a nonempty subset of the convex hull of the unknown source generating the original (nontrivial) measurement.

If we confine ourselves to looking for the convex source support corresponding to the original source generating the data and any convex domain enclosing the original domain, up to solving (2.2), we may assume that our domain of interest is a ball. After appropriate scaling, this ball can be considered to be the unit ball. This is the convention we will adopt for the rest of this work.

3 Constructive approximation of the CSS in 3D

Henceforth, we will assume that D is the unit ball. In this section, we will build a criterion for deciding if the convex source support $\mathscr{C}g$ lies in the intersection of D and a given closed ball $B \subset \mathbb{R}^3$. Since the closed balls enclosing a closed, convex set define that set uniquely, this provides a tool for reconstructing $\mathscr{C}g$.

Let $F \in \mathscr{E}'_\diamond(D) \subset \mathscr{E}'_\diamond(B_\rho)$, $\rho \geq 1$, be a fixed but unknown source and interpret $g = LF$ and $g^\rho = L_\rho F$ as functions of the polar $\theta \in [0,\pi]$ and the azimuthal $\phi \in (-\pi,\pi]$ angles. We denote the spherical harmonic coefficients of g and g^ρ by $\{g_{jk}\}$ and $\{g^\rho_{jk}\}$, respectively, i.e.,

$$g_{jk} = \int_{-\pi}^{\pi}\int_0^{\pi} g\,\overline{Y}_{jk}\sin\theta\,\mathrm{d}\theta\,\mathrm{d}\phi, \qquad g^\rho_{jk} = \int_{-\pi}^{\pi}\int_0^{\pi} g^\rho\,\overline{Y}_{jk}\sin\theta\,\mathrm{d}\theta\,\mathrm{d}\phi,$$

where $j \in \mathbb{N}_0$, $-j \leq k \leq j$, and $\{Y_{jk}\}$ are the (orthonormalized) complex spherical harmonics (cf. [1]) with $\overline{Y}_{jk}$ denoting the complex conjugate of Y_{jk}. This same subindex notation is used for the spherical harmonic coefficients of other functions as well. The following lemma provides a simple relation between the above sets of spherical harmonic coefficients; see [16, Lemma 3.1] for the related result in two dimensions. (Note that $g_{00} = g^\rho_{00} = 0$ due to the zero mean conditions of (1.1) and (2.3); this holds also for most of the other functions and distributions considered below.)

Lemma 3.1 *The spherical harmonic coefficients of g and g^ρ are related through*

$$g^\rho_{jk} = \frac{g_{jk}}{\rho^{j+1}}, \qquad j \in \mathbb{N},\ -j \leq k \leq j. \tag{3.1}$$

Proof In our concentric framework the solution of (2.2) can be given in spherical coordinates as

$$w_\rho(r,\theta,\phi) = \begin{cases} \sum_{j,k} g_{jk}\frac{j+1}{2j+1}\left(\rho^{-2j-1}-1\right)r^j\,Y_{jk}(\theta,\phi), & r \in (0,1), \\ \sum_{j,k} g_{jk}\left(\frac{j+1}{2j+1}\rho^{-2j-1}r^j + \frac{j}{2j+1}r^{-j-1}\right)Y_{jk}(\theta,\phi), & r \in (1,\rho). \end{cases}$$

In particular, according to the above considerations, we have

$$g^{\rho}(\theta,\phi) = w_{\rho}(\rho,\theta,\phi) = \sum_{j=1}^{\infty}\sum_{k=-j}^{j}\frac{g_{jk}}{\rho^{j+1}}Y_{jk}(\theta,\phi), \tag{3.2}$$

which completes the proof.

3.1 Concentric case

The first step in building our algorithm for reconstructing $\mathscr{C}g$ is introducing a test for deciding whether $\mathscr{C}g$ is enclosed by a closed ball of radius $0 < R < 1$ about the origin.

Theorem 3.1 *The function $g \in L^2_\diamond(\partial D)$ can be written as $g = LF$ for some $F \in \mathscr{E}'_\diamond(D)$ supported in $\overline{B}_R \subset D$ if and only if*

$$\sum_{j=1}^{\infty}\frac{j^m}{R^{2j}}\sum_{k=-j}^{j}|g_{jk}|^2 < \infty, \tag{3.3}$$

for some $m \in \mathbb{Z}$.

Proof The claim follows from a similar argumentation as in [15, Lemma 5.1], which is the corresponding result in two dimensions. Therefore, we present here only the general line of reasoning and skip some of the details.

Assume that there exists $F \in \mathscr{E}'_\diamond(D)$ with $\operatorname{supp} F \subset \overline{B}_R$ such that $g = u|_{\partial D}$, where u solves the source problem (1.1). As the potential u belongs to $H^l(D)$ for some $l \in \mathbb{Z}$, it follows from [24, Chapter 2, Theorems 6.5 and 7.3] that $\psi := (u|_{D\setminus\overline{B}_R})|_{\partial B_R}$ is well defined and belongs to $H^{l-1/2}(\partial B_R)$. We denote the spherical harmonic coefficients of ψ by

$$\psi_{jk} = \int_{-\pi}^{\pi}\int_0^{\pi} u(R,\theta,\phi)\overline{Y}_{jk}(\theta,\phi)\sin\theta\,\mathrm{d}\theta\,\mathrm{d}\phi, \qquad j \in \mathbb{N}_0,\ -j \le k \le j,$$

where the integral should be understood in the sense of dual evaluation between distributions and smooth functions. By using the unique solvability of the boundary value problem (cf. [24, Chapter 2, Remark 7.2])

$$\Delta w = 0 \quad \text{in } D\setminus\overline{B}_R, \qquad \frac{\partial w}{\partial \nu} = 0 \quad \text{on } \partial D, \qquad w = \psi \quad \text{on } \partial B_R \tag{3.4}$$

in $H^l(D\setminus\overline{B}_R)$, it is easy to see that we have the representation

$$u(r,\theta,\phi) = \sum_{j,k}\frac{\psi_{jk}}{(j+1)R^j + jR^{-j-1}}\big((j+1)r^j + jr^{-j-1}\big)Y_{jk}(\theta,\phi), \tag{3.5}$$

for $R < r \le 1$. In particular, we deduce that

$$|g_{jk}| = \frac{(2j+1)|\psi_{jk}|}{(j+1)R^j + jR^{-j-1}} \le CR^{j+1}|\psi_{jk}|, \qquad j \in \mathbb{N},\ -j \le k \le j.$$

As a consequence,

$$\sum_{j=1}^{\infty} \frac{j^{2l-1}}{R^{2j}} \sum_{k=-j}^{j} |g_{jk}|^2 \le CR^2 \sum_{j=1}^{\infty} j^{2l-1} \sum_{k=-j}^{j} |\psi_{jk}|^2 \le C\|\psi\|^2_{H^{l-1/2}(\partial B_R)} < \infty,$$

where the second to last inequality follows, e.g., from [24, Chapter 1, Remark 7.6] and $C > 0$ is a generic constant. This proves the 'only if' part of the claim.

Suppose next that (3.3) holds for some $m \in \mathbb{Z}$. Without loss of generality, we may assume that $m = -2l-1$ for some $l \in \mathbb{N}_0$. Let us consider the distribution

$$u(r,\theta,\phi) = \sum_{j=1}^{\infty} \sum_{k=-j}^{j} \frac{g_{jk}}{2j+1} \big((j+1)r^j + jr^{-j-1}\big) Y_{jk}(\theta,\phi), \qquad r \in (R,1).$$

It is easy to see that u has the Cauchy data $(g,0)$ on ∂D. Moreover, it follows from (3.3) that u is well defined and harmonic in $D \setminus \overline{B}_R$ and that the trace of u on ∂B_R,

$$u(R,\theta,\phi) = \sum_{j=1}^{\infty} \sum_{k=-j}^{j} \frac{g_{jk}}{2j+1} \big((j+1)R^j + jR^{-j-1}\big) Y_{jk}(\theta,\phi),$$

belongs to $H^{-l-1/2}(\partial B_R)$. Due to the well posedness of the boundary value problem (3.4), we thus deduce that $u \in H^{-l}(D \setminus \overline{B}_R)$. By continuing u as zero to B_R and setting $F = \Delta u \in H^{-l-2}(D) \cap \mathscr{E}'_\diamond(D)$, we have constructed a source that is supported on $\partial B_R \subset \overline{B}_R$ and satisfies $LF = g$. This completes the proof.

The test of Theorem 3.1 carries easily over to the case of the propagated data g^ρ and the extended domain B_ρ.

Corollary 3.1 *The function $g^\rho \in L^2_\diamond(\partial B_\rho)$ can be written as $g^\rho = L_\rho F$ for some $F \in \mathscr{E}'_\diamond(B_\rho)$ supported in $\overline{B}_R \subset B_\rho$ if and only if*

$$\sum_{j=1}^{\infty} \frac{j^m}{(R/\rho)^{2j}} \sum_{k=-j}^{j} |g^\rho_{jk}|^2 < \infty, \tag{3.6}$$

for some $m \in \mathbb{Z}$.

Proof The claim follows from a simple scaling argument.

In the following subsection, we will employ Kelvin transforms to deal with the case when the test ball is not centered at the origin. Although Kelvin transforms do preserve harmonicity, they differ from the conformal mappings of a two-dimensional space in the sense that Kelvin transforms do not retain homogeneous Neumann boundary conditions. Hence, we must consider the case of nonhomogeneous Neumann data before moving forward.

Corollary 3.2 *Let $(g^*, f^*) \in L^2_\diamond(\partial B_\rho) \times L^2_\diamond(\partial B_\rho)$ be a given pair of Cauchy data on ∂B_ρ. There exists a source $F^* \in \mathscr{E}'_\diamond(B_\rho)$ supported in $\overline{B}_R \subset B_\rho$ and a potential $u^* \in \cup_{m\in\mathbb{Z}} H^m(B_\rho)$ such that*

$$\Delta u^* = F^* \quad \text{in } B_\rho, \qquad u^* = g^* \quad \text{on } \partial B_\rho, \qquad \frac{\partial u^*}{\partial \nu} = f^* \quad \text{on } \partial B_\rho \tag{3.7}$$

if and only if

$$\sum_{j=1}^{\infty} \frac{j^m}{(R/\rho)^{2j}} \sum_{k=-j}^{j} |j g^*_{jk} - \rho f^*_{jk}|^2 < \infty,$$

for some $m \in \mathbb{Z}$.

Proof Let us introduce the auxiliary potential

$$v(r,\theta,\phi) = \rho \sum_{j=1}^{\infty} \frac{(r/\rho)^j}{j} \sum_{k=-j}^{j} f^*_{jk} Y_{jk}(\theta,\phi), \tag{3.8}$$

which represents the unique solution of the Neumann boundary value problem

$$\Delta v = 0 \quad \text{in } B_\rho, \qquad \frac{\partial v}{\partial \nu} = f^* \quad \text{on } \partial B_\rho, \qquad \int_{\partial B_\rho} v \,\mathrm{d}s = 0 \tag{3.9}$$

in $H^1(B_\rho)$. Due to the linearity of the considered partial differential equations, there exists a solution $u^* \in \cup_{m\in\mathbb{Z}} H^m(D)$ of (3.7) if and only if $L_\rho F^* = g^* - v|_{\partial B_\rho}$. In consequence, the claim follows from Corollary 3.1 and the representation (3.8).

3.2 Nonconcentric case

Let $B \subset \mathbb{R}^3$ be an arbitrary closed ball of radius $R > 0$, and choose a large enough radius $\rho \geq 1$ so that B_ρ contains B. Without loss of generality, we may assume that the center of B lies on the positive x_1-axis and denote it by $(c,0,0)$; if this was not the case, we could rotate the coordinate system. Let us introduce the mapping

$$\mathscr{I} = \mathscr{I}_{B,\rho} : \mathbb{R}^3 \cup \infty \to \mathbb{R}^3 \cup \infty, \qquad x \mapsto m + \frac{b^2}{|x-m|^2}(x-m),$$

where we choose

$$m = (a,0,0), \qquad b = \sqrt{a^2 - \rho^2},$$

and

$$a = \frac{\rho^2 + c^2 - R^2}{2c} + \sqrt{\left(\frac{\rho^2 + c^2 - R^2}{2c}\right)^2 - \rho^2}\,.$$

Notice that $a > \rho$ because $R < \rho - c$ by assumption. This means, in particular, that $b > 0$ is well-defined and $m \notin B_\rho$.

The map $\mathscr{I}$ is an *inversion* with respect to the sphere of radius b centered at $m \in \mathbb{R}^3$ [2, Definition 1.6.2], i.e., $\mathscr{I}(x)$ lies on the line passing through x and m, and

$$|x-m||\mathscr{I}(x)-m| = b^2, \qquad x \neq m. \tag{3.10}$$

In particular, $\mathscr{I}$ is its own inverse and its Jacobian determinant is given by

$$\det \mathscr{I}'(x) = -\frac{b^6}{|x-m|^6}, \qquad x \neq m. \tag{3.11}$$

Moreover, somewhat tedious but straightforward calculations show that

$$\mathscr{I}(\overline{B}_\rho) = \overline{B}_\rho \qquad \text{and} \qquad \mathscr{I}(B) = \overline{B}_{R^*},$$

where

$$R^* = \sqrt{\frac{a(\rho^2 - ac)}{a-c}}.$$

We define the (distributional) *Kelvin transform* $\mathscr{H} = \mathscr{H}_{B,\rho} : \mathscr{D}'(B_\rho) \to \mathscr{D}'(B_\rho)$ via

$$\langle \mathscr{H} v, \varphi \rangle = \left\langle v, \frac{b^5}{|\cdot - m|^5} \varphi \circ \mathscr{I} \right\rangle, \qquad \varphi \in \mathscr{D}(B_\rho). \tag{3.12}$$

A straightforward calculation shows that $\mathscr{H}$ is its own inverse. Away from the singular support of v, i.e., where v can be represented by a smooth function, the above dual evaluation can be interpreted as an integral. Consequently, the change of variables $y = \mathscr{I}(x)$ results in (cf. (3.10) and (3.11))

$$\mathscr{H} v(x) = \frac{b}{|x-m|} v(\mathscr{I}(x)), \qquad \mathscr{I}(x) \notin \operatorname{sing\,supp} v, \tag{3.13}$$

which coincides with the traditional Kelvin transform of v (cf. [2, Section 1.6]). Notice also that

$$(\Delta(\mathscr{H} v))(x) = \frac{b^5}{|x-m|^5} (\Delta v) \circ \mathscr{I}(x), \qquad x \in B_\rho, \tag{3.14}$$

for any $v \in C^2(B_\rho)$ (cf., e.g., [2, Theorem 1.6.3]).

Theorem 3.2 *The function $g^\rho \in L^2_\diamond(\partial B_\rho)$ can be written as $g^\rho = L_\rho F$ for some $F \in \mathscr{E}'_\diamond(B_\rho)$ supported in B if and only if there exists a source $F^* \in \mathscr{E}'_\diamond(B_\rho)$ supported in $\overline{B}_{R^*}$ and a potential $u^* \in \cup_{m\in\mathbb{Z}} H^m(B_\rho)$ satisfying*

$$\Delta u^* = F^* \quad \text{in } B_\rho, \qquad u^* = g^* \quad \text{on } \partial B_\rho, \qquad \frac{\partial u^*}{\partial \nu} = f^* \quad \text{on } \partial B_\rho \tag{3.15}$$

for

$$g^*(x) = \mathscr{H} g^\rho(x) \qquad \text{and} \qquad f^*(x) = -\frac{1}{\rho} \frac{x \cdot (x-m)}{|x-m|^2} \mathscr{H} g^\rho(x), \tag{3.16}$$

where $\mathscr{H} g^\rho(x) = \mathscr{H}_{B,\rho} g^\rho(x)$, $x \in \partial B_\rho$, is defined by formula (3.13).

Proof We begin by assuming that there exists $F \in \mathscr{E}'_\diamond(B_\rho)$ with $\operatorname{supp} F \subset B$ such that $g^\rho = u|_{\partial B_\rho}$, where u is the solution of the source problem (2.3). Let us consider the modified potential $u^* = \mathscr{H} u$, where $\mathscr{H} = \mathscr{H}_{B,\rho}$ is defined by (3.12). Since u is smooth near the boundary ∂B_ρ due to the regularity theory of elliptic partial differential equations [24], u^* can be represented by the formula (3.13) in some (interior) neighborhood of ∂B_ρ. Thus, a straightforward calculation utilizing the identity $\mathscr{I}(\partial B_\rho) = \partial B_\rho$ shows that u^* satisfies the boundary conditions of (3.15). Moreover, distributional differentiation and (3.14) give

$$\langle \Delta u^*, \varphi \rangle = \langle u^*, \Delta\varphi \rangle = \left\langle u, \frac{b^5}{|\cdot - m|^5} (\Delta\varphi) \circ \mathscr{I}(\cdot) \right\rangle = \langle u, \Delta(\mathscr{H}\varphi) \rangle = \langle F, \mathscr{H}\varphi \rangle$$

for all $\varphi \in \mathscr{D}(B_\rho)$. Since $\operatorname{supp} \mathscr{H}\varphi = \mathscr{I}(\operatorname{supp}\varphi)$ and $\operatorname{supp} F \subset B$, the dual evaluation $\langle \Delta u^*, \varphi \rangle$ vanishes if $\operatorname{supp}\varphi \subset B_\rho \setminus \overline{B}_{R^*}$, which means that the source $F^* = \Delta u^* \in \mathscr{E}'(B_\rho)$ is supported in $\overline{B}_{R^*}$. Finally, using the harmonicity of

$$(\mathscr{H}\mathbf{1})(x) = \frac{b}{|x-m|}, \qquad x \in B_\rho,$$

we deduce that

$$\langle F^*, \mathbf{1} \rangle = \langle u, \Delta(\mathscr{H}\mathbf{1}) \rangle = 0,$$

which shows that $F^* \in \mathscr{E}'_\diamond(B_\rho)$.

Assume next that there exists $F^* \in \mathscr{E}'_\diamond(B_\rho)$, with $\operatorname{supp} F^* \subset \overline{B}_{R^*}$, and a potential $u^* \in \cup_{m\in\mathbb{Z}} H^m(B_\rho)$ that satisfies (3.15)–(3.16). Let us consider the distribution $u = \mathscr{H} u^*$. We can use the smoothness of u^* near the boundary ∂B_ρ and (3.13) to deduce that

$$u = g^\rho \quad \text{on } \partial B_\rho \qquad \text{and} \qquad \frac{\partial u}{\partial \nu} = 0 \quad \text{on } \partial B_\rho.$$

Moreover, in exactly the same way as above it follows that

$$\langle \Delta u, \varphi \rangle = \langle F^*, \mathscr{H}\varphi \rangle$$

for all $\varphi \in \mathscr{D}(B_\rho)$. Hence, the source $F = \Delta u \in \mathscr{E}'(B_\rho)$ is supported in $I(\operatorname{supp} F^*) \subset B$. Because F is mean-free due to the homogeneous Neumann boundary condition of u on ∂B_ρ, it follows from the corresponding Dirichlet boundary condition that $L_\rho F = g^\rho$, which completes the proof.

The following corollary is the main building block of the reconstruction algorithm to be introduced in Section 4 below.

Corollary 3.3 *Let $g \in \mathscr{R}(L)$. Then, we have $\mathscr{C} g = \mathscr{C}_\rho g^\rho \subset B \cap D$ if and only if*

$$\sum_{j=1}^{\infty} \frac{\rho^{2j}}{(R^* + \varepsilon)^{2j}} \sum_{k=-j}^{j} |j g^*_{jk} - \rho f^*_{jk}|^2 < \infty, \tag{3.17}$$

for every $\varepsilon > 0$. Here, g^* and f^* are defined as in Theorem 3.2.

Proof The assertion follows by combining the line of reasoning leading to [15, Corollary 5.4] with Theorem 2.2, Corollary 3.2 and Theorem 3.2.

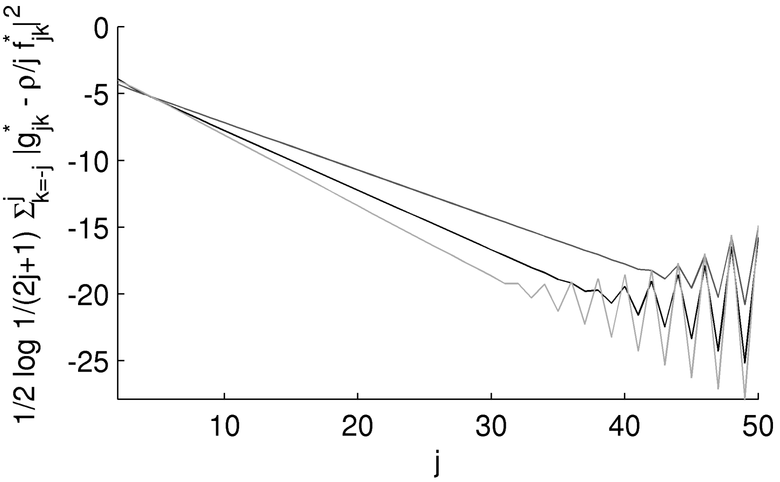

Fig. 4.1 Logarithms of the expression (4.1) as functions of the index j for a fixed boundary potential g and $\rho = 1.4$. Three different Kelvin transforms were used to obtain three sets of spherical harmonic coefficients.

4 Algorithmic implementation

In order to employ the convergence test (3.17) in practice for some $g = LF$, a computational algorithm must be devised. A suitable method for a two-dimensional setting was proposed in [16], where a test involving Fourier coefficients of boundary data was handled as a geometric series obtained through logarithmic regression. A similar approximation is a viable option also in our three-dimensional framework: The logarithms of

$$\frac{1}{2j+1}\sum_{k=-j}^{j}\left|g_{jk}^{*}-\frac{\rho}{j}f_{jk}^{*}\right|^{2} \tag{4.1}$$

typically exhibit a linear behavior as a function of j; see Figure 4.1. As a motivation of this observation, notice that if $f^* = 0$, the sum (4.1) simplifies to the mean of the spherical harmonic coefficients of g^* corresponding to the spatial frequency j, which is analogous to the basic idea of the two-dimensional algorithm in [16]; see also [5] from which such a linear regression idea stems. Thus, substituting the approximation

$$\frac{1}{2}\log\frac{1}{2j+1}\sum_{k=-j}^{j}\left|g_{jk}^{*}-\frac{\rho}{j}f_{jk}^{*}\right|^{2}\approx aj+b, \quad j\in\mathbb{N}, \tag{4.2}$$

in (3.17) yields the series

$$\sum_{j=1}^{\infty} j^{2}(2j+1)\frac{\rho^{2j}e^{2(aj+b)}}{(R^{*}+\varepsilon)^{2j}}, \tag{4.3}$$

which converges for all $\varepsilon > 0$ if and only if $R^* \geq \rho e^{a}$. Because numerical inaccuracies render the high-frequency components unreliable (cf. Figure 4.1), it is imperative to choose a cut-off level beyond which the coefficients are discarded. In practice, the used indices are chosen on a case-specific manner through visual inspection.

Although the above procedure was derived to test if a given ball B contains $\mathscr{C}g$, it effectively applies the convergence test simultaneously to an infinite family of nested closed balls,

$$\{\mathscr{I}_{B,\rho}(\overline{B}_r) \subset \mathbb{R}^3 \mid 0 \leq r < \rho\}. \tag{4.4}$$

Indeed, the same inversion, i.e., $\mathscr{I}_{B,\rho} = \mathscr{I}_{B,\rho}^{-1}$, maps each ball in this family onto a closed concentric ball inside B_ρ, and thus the convergence test analogous to (4.3) for the ball $\mathscr{I}_{B,\rho}(\overline{B}_r)$ is obtained by replacing R^* in the denominator of (4.3) by r. In consequence, $\mathscr{C}g \subset \mathscr{I}_{B,\rho}(\overline{B}_r)$ if and only if $r \geq \rho e^a$ — under the courtesy of the assumption that (4.2) is exact. Obviously, this same reasoning remains valid in the degenerate case when the closed ball B parameterizing the used inversion is just a single point lying inside B_ρ, i.e., if we consider the inversion that maps $\overline{B}_\rho$ onto itself and some given point $z \in B_\rho$ to the origin. Such a mapping is obtained by setting $R = 0$ in the formulae of Section 3.2; by slight abuse of notation, we denote it by $\mathscr{I}_{z,\rho}$, and the corresponding cut-off radius by $R_0 = R_0(z,\rho) = \rho e^a$, where the decay rate $a \in \mathbb{R}$ is obtained from (4.2) for $\mathscr{I} = \mathscr{I}_{z,\rho}$ (cf. (3.14) and (3.16)). To decrease the number of free parameters, we only use inversions of this form in the following.

In our numerical algorithm, we fix $\rho > 1$, choose a discrete set of test points $Z \subset B_\rho$, and approximate the convex source support by

$$\mathscr{C}g \approx \bigcap_{z \in Z} \mathscr{I}_{z,\rho}(\overline{B}_{R_0(z,\rho)}). \tag{4.5}$$

Theoretically, it would be advantageous to include in Z points that lie far away from the origin: Then, larger balls would enter the intersection on the right-hand side of (4.5), and we would, in principle, obtain a better approximation of the convex set $\mathscr{C}g$. However, to make this possible, the parameter ρ would have to be large, which would make the algorithm more susceptible to (even numerical) noise since the high-frequency information in the original data g is strongly diluted when extended onto ∂B_ρ due to the ellipticity of the forward problem, cf. Lemma 3.1. According to our experience, choosing $\rho = 1.4$ and letting Z be an evenly distributed set of points on a sphere of radius 0.8 is a good compromise between theoretical accuracy and stability of the algorithm; in all numerical studies presented below, Z is composed of the vertices of a regular icosahedron, that is, 12 points. Take note that there is no reason for including points close to the origin in Z: The balls centered far away from the origin are — at least in theory — able to capture all features of the convex set $\mathscr{C}g$.

5 Numerical studies

For any given boundary potential $g = LF$, we employ two data sets of varying quality: they are called *ideal* and *realistic*, as explained in the following.

In order to find the limits for the functionality of our algorithm, we introduce *ideal* data: The propagated boundary potential g^ρ is simulated by directly solving the extended source problem (2.3). For each test point $z \in Z$, the value of g^ρ is evaluated at those points that are mapped by $\mathscr{I}_{z,\rho}$ onto a fixed Cartesian grid $\{\rho x_{jk}\}$ in spherical coordinates on ∂B_ρ, where $x_{jk} = (\sin\theta_j \cos\phi_k, \sin\theta_j \sin\phi_k, \cos\theta_j)$ with $\theta_j = \pi j/J$, $j = 1,\dots,J$, and $\phi_k = 2\pi k/K$, $k = 1,\dots,K$. Hence, the values of g^* and f^* are known on $\{\rho x_{jk}\}$ (cf. (3.14) and (3.16)), which makes the numerical computation of the spherical harmonic coefficients needed in (4.2) as stable as possible with the standard routines, and thus the corresponding reconstructions should be optimal. According to our experience, increasing the number of grid points further than $J = 50, K = 99$ does not affect the quality of reconstructions considerably; these values for J and K were used in all of the numerical examples.

Naturally, the above described ideal data cannot be obtained in real life: One cannot have direct access to values of the extended boundary potential g^ρ, but only to those of g, and, furthermore, the measured values of g are in practice corrupted by noise. Hence, we also consider *realistic* data: First, the point values of g are evaluated on the grid $\{x_{jk}\} \subset \partial D$. Second, a significant amount of noise is added to these point values, creating the realistic data set

$$g_n(x_{jk}) = g(x_{jk}) + 0.1 n_{jk} \max_{\nu,\mu} |g(x_{\nu\mu})|, \quad 1 \le j \le J, \quad 1 \le k \le K,$$

where $\{n_{jk}\}$ are realizations of a normally distributed random variable with zero mean and unit variance. To be able to use the algorithm of Section 4 with such data, we approximate the spherical harmonic coefficients of g from the noisy point values $\{g_n(x_{jk})\}$, and subsequently those of g^ρ with the help of (3.1). Finally, for each test point $z \in Z$ we evaluate $\mathscr{H}_{z,\rho} g^\rho$ on the grid $\{\rho x_{jk}\} \subset \partial B_\rho$ by approximating g^ρ with its truncated spherical harmonic expansion, which then makes it possible to compute the spherical harmonic coefficients of g^* and f^* (cf. (3.16)) needed in (4.2).

5.1 Inverse source problem

Let us first consider the actual inverse source problem for the Laplacian with two different sources. The first source is a sum of two dipoles

$$F_1 = \alpha \cdot \nabla \delta_p + \beta \cdot \nabla \delta_q$$

where $p = (0.2, 0.2, 0.2)$, $q = (-0.5, 0, 0)$ and δ_y denotes the delta distribution located at some point $y \in D$. The dipole moments are chosen to be of different orders of magnitude, namely $\alpha = (0,1,0)$ and $\beta = 10^{-2}(1,0,0)$, in order to test how well the proposed algorithm is able to detect small changes in the source term. With the help of the Neumann function for the Laplacian in the unit ball [31]

$$N(x,y) = \frac{1}{4\pi}\left(\frac{1}{|x-y|} + \frac{1}{\left||y|x - \frac{y}{|y|}\right|} + \log\left(\frac{2}{1 - x\cdot y + \left||y|x - \frac{y}{|y|}\right|}\right)\right), \qquad (5.1)$$

the solution of (1.1) corresponding to F_1 can be written as

$$u_1(x) = -\alpha \cdot \nabla_x N(x,p) - \beta \cdot \nabla_x N(x,q), \qquad x \in D, \qquad (5.2)$$

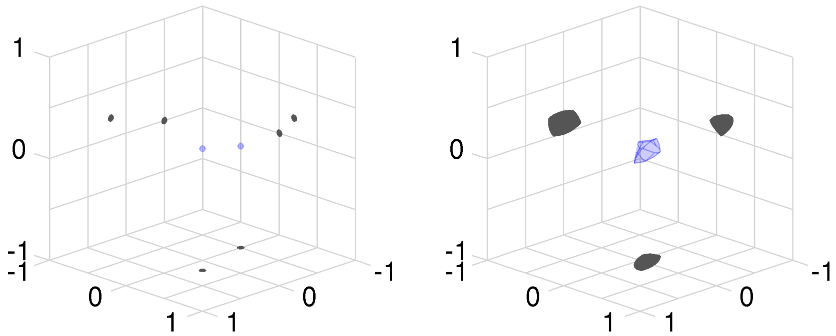

Fig. 5.1 Left: The locations of the dipoles composing the source F_1. Right: The reconstruction of the corresponding CSS from ideal data. In these and all the following images, the third coordinate x_3 corresponds to the vertical direction, and the x_1 and x_2 axes are oriented so that (x_1, x_2, x_3) is a right-handed system.

where the gradients act on the first variable. The corresponding solution of (2.3), which is needed when simulating ideal data, is obtained by replacing $N(\cdot,\cdot)$ in (5.2) with the the Neumann function for B_ρ, i.e.,

$$N_\rho(x,y) = \frac{1}{\rho} N(x/\rho, y/\rho), \qquad x,y \in B_\rho.$$

The second investigated source is a linear function supported within the rectangular cuboid E depicted in the left-hand image of Figure 5.2,

$$F_2(x) = x_1 \chi_E(x),$$

where χ_E is the characteristic function of E. Notice that F_2 is mean-free because E is symmetric with respect to the (x_2, x_3) coordinate plane. Simulation of the boundary data corresponding to F_1 is trivial since the associated potentials are known explicitly. The boundary data corresponding to $F = F_2$ is generated by solving (1.1), or (2.3) if ideal data is considered, using the finite element method.

The left-hand image of Figure 5.1 depicts the locations of the two dipoles composing the source F_1; the image also shows the projections of the dipoles onto the coordinate planes, which is a convention that is used in all of our figures. The right-hand image illustrates the corresponding reconstruction from ideal data. Compared to the actual CSS, which is in this case the line segment between the points p and q (cf. [15, Example 3.1]), the reconstruction is not totally accurate: It covers the stronger dipole but extends only half way to the direction of the weaker one. Moreover, the reconstructed CSS is too roundish. The first of these two flaws could be fixed by omitting some lowest frequencies j in the linear regression model (4.2): According to our experience, only the stronger dipole is visible in the spherical harmonic coefficients corresponding to low spatial frequencies whereas high-frequency coefficients contain information about both dipoles. On the other hand, the second flaw could be tackled by increasing the radius of the extended domain B_ρ, which would enable the use of larger balls in (4.5) and allow, in principle, a more accurate reconstruction. Unfortunately, this would also make the algorithm more sensitive to noise.

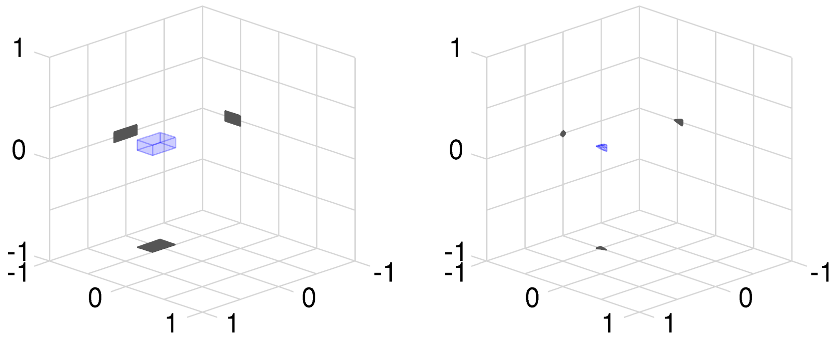

Fig. 5.2 Left: The rectangular cuboid E that is the support of the source F_2. Right: The reconstruction of the corresponding CSS from ideal data.

Because we want our reconstruction method to be independent of the properties of the source in question and to function in the same form for both ideal and realistic data, we have refrained from making these 'improvements' to our algorithm.

The reconstruction corresponding to the second source F_2 and ideal data is shown in the right-hand image of Figure 5.2; recall that the left-hand image depicts the support of F_2, i.e., E. Although the reconstruction is smaller than E, its location is accurate.

Figure 5.3 shows the reconstructions provided by our algorithm for realistic data and the two sources F_1 and F_2 introduced above. In comparison to the ideal case, the most apparent deterioration is that the reconstruction corresponding to F_1 is no more affected notably by the dipole with the smaller moment at q. This is not very surprising as the influence that the weaker dipole has on the boundary measurement is easily covered in noise. Although neither of the two reconstructions captures any information on the size or the shape of the corresponding source, one can argue that the algorithm still provides some information on the approximate location of the target source in both cases. In fact, it seems that the algorithm is relatively robust with

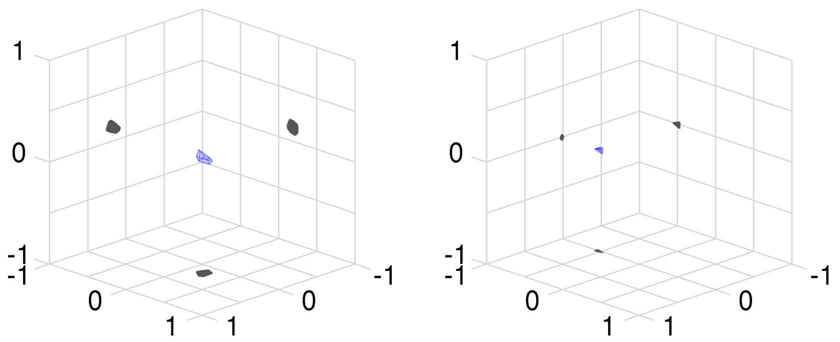

Fig. 5.3 Reconstructions corresponding to realistic data. Left: The target source F_1 composed of two dipoles. Right: The target source F_2 supported on the rectangular cuboid E.

respect to measurement noise as the reconstruction corresponding to F_2 is not notably affected by the 10% noise level in the data.

5.2 Electrical impedance tomography

Let us consider the elliptic boundary value problem

$$\nabla\cdot(\sigma\nabla v)=0 \quad \text{in } D, \qquad \frac{\partial v}{\partial \nu}=\delta_{y_+}-\delta_{y_-} \quad \text{on } \partial D, \qquad \int_{\partial D} v\,\mathrm{d}s=0, \tag{5.3}$$

where $y_+,y_-\in\partial D$, $y_+\neq y_-$ are fixed current source locations and the distributions $\delta_{y_\pm}$ are Dirac deltas on ∂D. In the numerical experiments below, we pick $y_+=(1,0,0)$ and $y_-=(-1,0,0)$. The conductivity $\sigma\in L^\infty(D)$, $\sigma\geq c>0$, is assumed to be such that $\Omega:=\operatorname{supp}(\sigma-1)$ is a compact subset of D, i.e., $\sigma=1$ in some interior neighborhood of the boundary ∂D. Take note that the third condition of (5.3) should, in fact, be understood as dual evaluation between the trace $v|_{\partial D}$ and the unit function on ∂D (cf. [24, Chapter 2, Section 7]). Since $\delta_{y_\pm}\in H^{-1-\varepsilon}(\partial D)$, $\varepsilon>0$, it follows from the the material in [17, Appendix] that (5.3) has a unique solution in $H^{1/2-\varepsilon}(D)\cap H^1_{\mathrm{loc}}(D)$; see also [24, Chapter 2, Remark 7.2]. The EIT problem considered in this work is to deduce information on the inhomogeneity Ω from the value of the electromagnetic potential v measured on ∂D.

Let v_0 be the reference potential, i.e., the solution of (5.3) corresponding to $\sigma\equiv 1$. For example, the same reasoning as in [18, Proof of Theorem A.2] shows that v_0 can be written explicitly as

$$v_0(x)=N(x,y_+)-N(x,y_-), \qquad x\in D,$$

where $N(\cdot,\cdot)$ is the Neumann function for the Laplacian in the unit ball given by (5.1). It follows trivially that the relative potential $w=v-v_0$ is the solution of (1.1) for

$$F=F(y_\pm,\sigma)=\Delta v\in\mathscr{E}'_\diamond(D)\cap H^{-1}(D),$$

which is supported in Ω. Hence, setting $g=w|_{\partial D}$, we may use the algorithm described above to approximate the corresponding convex source support $\mathscr{C}g$, which is a nonempty subset of the convex hull of the inhomogeneity Ω (cf. [16]) — assuming that the measured relative boundary potential g is nontrivial.

In practice, the data g can be collected with three (infinitely small) electrodes (cf. [14]): Constant flux of current is maintained between two electrodes at fixed locations y_+ and y_-. Meanwhile, the third electrode, which is moved along ∂D and not used for current injection, measures the boundary potential. Naturally, one needs also to be able to carry out this same measurement without the inhomogeneity Ω in D or, alternatively, compute the reference boundary potential $v_0|_{\partial D}$ numerically.

Before moving on to the numerical examples, let us consider briefly how the relative potential w can be simulated numerically. By applying the differential operator $\nabla\cdot(\sigma\nabla\cdot)$ on w, it follows that

$$\nabla\cdot(\sigma\nabla w)=-\nabla\cdot(\sigma\nabla v_0) \quad \text{in } D, \qquad \frac{\partial w}{\partial \nu}=0 \quad \text{on } \partial D, \qquad \int_{\partial D} w\,\mathrm{d}s=0. \tag{5.4}$$

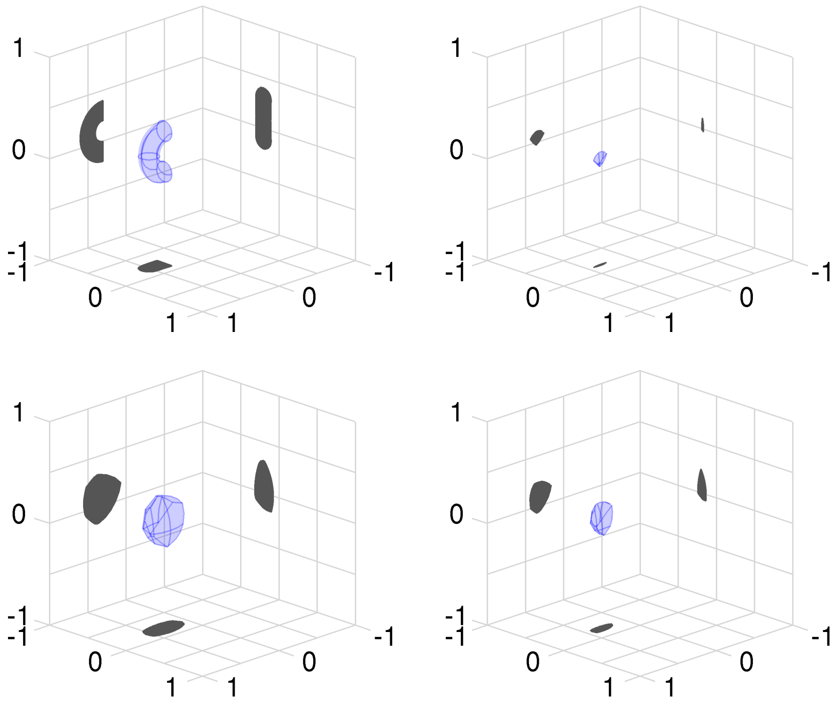

Fig. 5.4 Top left: The semitoroidal inclusion. The other three images show reconstructions from ideal data corresponding to different conductivity profiles inside the inclusion. Top right: $\sigma \equiv 2$ in Ω. Bottom left: $\sigma(x) = 1 + (x_3 - 0.1)/0.6$ in Ω. Bottom right: $\sigma(x) = 1 + 0.5\cos(10x_1)$ in Ω.

Since $\sigma = 1$ in some interior neighborhood of ∂D and v_0 is smooth in the interior of D, the source term

$$-\nabla \cdot (\sigma \nabla v_0) = \nabla \cdot ((1-\sigma)\nabla v_0)$$

belongs to $\mathscr{E}'_\diamond(D) \cap H^{-1}(D)$. Hence, standard variational argumentation (cf., e.g., [7]) shows that (5.4) has a unique solution, i.e., the relative potential w, which is the unique solution of the problem

$$\int_D \sigma \nabla w \cdot \nabla \phi \, \mathrm{d}x = \int_D (1-\sigma)\nabla v_0 \cdot \nabla \phi \, \mathrm{d}x \qquad \text{for all } \phi \in H^1(D) \qquad (5.5)$$

among the elements of $H^1(D)$ having zero mean on ∂D. The relative boundary potentials needed for the numerical studies below are simulated by solving the variational equation (5.5) — or in the case of ideal data the one obtained by replacing D with B_ρ everywhere in (5.5) — using the commercial finite element solver Comsol.

Let us first consider the case that the inclusion Ω is the semitorus depicted in the top left image of Figure 5.4. The other three images of Figure 5.4 show the reconstructions produced by our algorithm for ideal data and three different conductivity distributions inside the inhomogeneity: In the top right image the conductivity of the inclusion is identically 2, in the bottom left image $\sigma(x) = 1 + (x_3 - 0.1)/0.6$ in Ω,

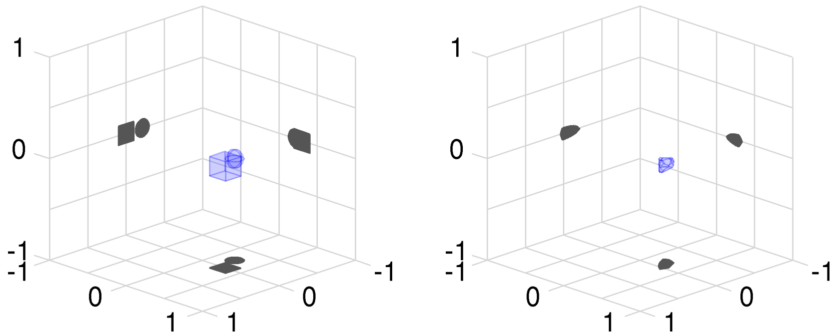

Fig. 5.5 Left: The inhomogeneity composed of a ball and a cube with conductivities 0.5 and 2, respectively. Right: The reconstruction of the corresponding CSS from ideal data.

and in the bottom right image $\sigma(x) = 1 + 0.5\cos(10x_1)$ in Ω. Note that the semitorus lies between the planes $x_3 = -0.2$ and $x_3 = 0.4$, and thus all of these conductivity distributions take values in the range $[0.5, 2]$. The algorithm finds the location of the inhomogeneity accurately in all three cases. However, while the reconstructions corresponding to the first and third conductivity profiles are too small, for the second profile the size of the inclusion is reproduced accurately. According to this test, the reconstruction method is not sensitive only to the shape of the inclusion but also to the conductivity distribution inside the inclusion.

Our second inhomogeneity is the disconnected union of a small ball and a cube shown in the left-hand image of Figure 5.5. The conductivity inside the ball is identically 0.5 and inside the cube identically 2. The reconstruction of the corresponding CSS, obtained using ideal data, is presented in the right-hand image of Figure 5.5. Once again, the algorithm finds the location of the inhomogeneity accurately, but the reconstruction is slightly too small.

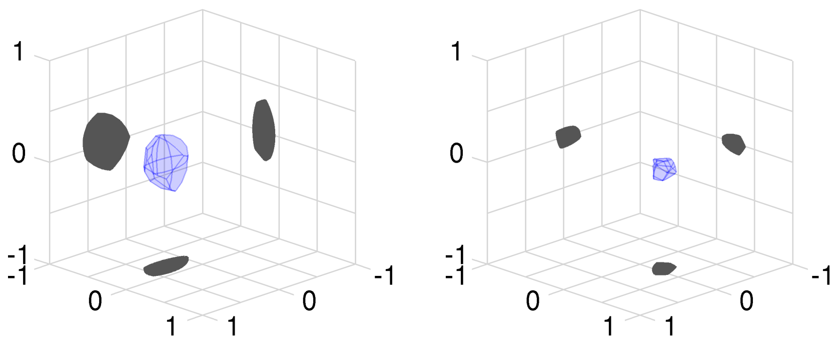

Fig. 5.6 Reconstructions corresponding to realistic data. Left: The semitoroidal inclusion with the conductivity profile $\sigma(x) = 1 + (x_3 - 0.1)/0.6$. Right: The inhomogeneity composed of a ball and a cube with conductivities 0.5 and 2, respectively.

Our final numerical test considers locating the above introduced inclusions, i.e., the semitorus and the union of the small ball and cube, from realistic data; for the semitorus we choose the conductivity profile $\sigma(x) = 1 + (x_3 - 0.1)/0.6$. The results are illustrated in Figure 5.6. As for the inverse source problem with realistic data, the reconstructions in Figure 5.6 point out the approximate locations of the corresponding inhomogeneities but do not reveal any further details. Actually, the information contents of these reconstructions are, arguably, approximately the same as of the corresponding ones for ideal data in Figures 5.4 and 5.5. This is further evidence for the robustness of our algorithm with respect to measurement noise.

Although our algorithm does not reconstruct the conductivity, but only aims at revealing information about the support of a conductivity inhomogeneity, it should be noted that our algorithm also uses far less data than most other direct reconstruction methods for EIT: Here, we work with only one pair of boundary current and potential, not with the whole Neumann-to-Dirichlet map (cf., e.g., [3, 29]).

6 Concluding remarks

We have introduced a numerical technique for reconstructing the convex source support corresponding to the Poisson equation in bounded three-dimensional domains. The method is based on replacing the Möbius transformations needed in the corresponding two-dimensional algorithm [16] by inversions with respect to suitable spheres and introducing the associated Kelvin transforms. The functionality of the algorithm was demonstrated by applying it both to the actual inverse source problem and to the obstacle problem in EIT with only one relative boundary potential as measurements.

References

1. Arfken, G.: Mathematical Methods for Physicists, Academic Press, New York (1970)
2. Armitage, D. H., Gardiner, S. J.: Classical Potential Theory, Springer-Verlag, London (2001)
3. Borcea, L.: Electrical impedance tomography, Inverse Problems **18**, R99–R136 (2002)
4. Bourgeois, L., Chambeyron, C., Kusiak, S.: Locating an obstacle in a 3D finite depth ocean using the convex scattering support, J. Comput. Appl. Math. **204**, 387–399 (2007)
5. Brühl, M., Hanke, M.: Numerical implementation of two noniterative methods for locating inclusions by impedance tomography, Inverse Problems **16**, 1029–1042 (2000)
6. Cheney, M., Isaacson, D., Newell, J. C.: Electrical impedance tomography, SIAM Rev. **41**, 85–101 (1999)
7. Dautray, R., Lions, J.-L.: Mathematical Analysis and Numerical Methods for Science and Technology, vol. 2, Springer-Verlag, Berlin (1988)
8. El Badia, A., Ha Duong, T.: Some remarks on the problem of source identification from boundary measurements, Inverse Problems **14**, 883–891 (1998)
9. El Badia, A., Ha Duong, T.: An inverse source problem in potential analysis, Inverse Problems **16**, 651–663 (2000)
10. El Badia, A.: Inverse source problem in an anisotropic medium by boundary measurements, Inverse Problems **21**, 1487–1506 (2005)
11. Haddar, H., Kusiak, S., Sylvester, J.: The convex back-scattering support, SIAM J. Appl. Math. **66**, 591–615 (2005)
12. Hakula, H., Hyvönen, N.: Two noniterative algorithms for locating inclusions using one electrode measurement of electric impedance tomography, Inverse Problems **24**, 055018 (2008)

13. Hämäläinen, M., Hari, R., Ilmoniemi, R. J., Knuutila, J., Lounasmaa, O. V.: Magnetoencephalography — theory, instrumentation, and applications to noninvasive studies of signal processing in the human brain, Rev. Mod. Phys. **65**, 413–497 (1993)
14. Hanke, M., Harrach, B., Hyvönen, N.: Justification of point electrode models in electrical impedance tomography, accepted to Math. Models Methods Appl. Sci.
15. Hanke, M., Hyvönen, N., Lehn, M., Reusswig, S.: Source supports in electrostatics, BIT **48**, 245–264 (2008)
16. Hanke, M., Hyvönen, N., Reusswig, S.: Convex source support and its application to electric impedance tomography, SIAM J. Imaging Sci. **1**, 364–378 (2008)
17. Hanke, M., Hyvönen, N., Reusswig, S.: Convex backscattering support in electric impedance tomography, Numer. Math., DOI:10.1007/s00211-010-0320-9 (2010)
18. Harhanen, L., Hyvönen, N.: Convex source support in half-plane, Inverse Probl. Imaging **4**, 429–448 (2010)
19. Isakov, V.: Inverse Source Problems, American Mathematical Society, Providence (1990)
20. Isakov, V.: Inverse Problems for Partial Differential Equations, 2. ed, Springer, New York (2006)
21. Kang, H., Lee, H.: Identification of simple poles via boundary measurements and an application of EIT, Inverse Problems **20**, 1853–1863 (2004)
22. Kusiak, S., Sylvester, J.: The scattering support, Comm. Pure Appl. Math. **56**, 1525–1548 (2003)
23. Kusiak, S., Sylvester, J.: The convex scattering support in a background medium, SIAM J. Math Anal. **36**, 1142–1158 (2005)
24. Lions, J. L., Magenes, E.: Non-Homogeneous Boundary Value Problems and Applications, vol I, Springer-Verlag, Berlin (1972)
25. Potthast, R., Sylvester, J., Kusiak, S.: A ‘range test’ for determining scatterers with unknown physical properties, Inverse Problems **19**, 533–547 (2003)
26. Schweickert, E.: Characterisierung des diskoidalen Quellträgers der Poissongleichung in der Kugel, Master’s Thesis, Johannes Gutenberg–Universität Mainz, Mainz (2008) (in German)
27. Sylvester, J., Kelly, J.: A scattering support for broadband sparse far field measurements, Inverse Problems **21**, 759–771 (2005)
28. Sylvester, J.: Notions of support for far fields, Inverse Problems **22**, 1273–1288 (2006)
29. Uhlmann, G.: Electrical impedance tomography and Calderón’s problem, Inverse Problems **25**, 123011 (2009)
30. Vessella, S.: Locations and strengths of point sources: stability estimates, Inverse Problems **8**, 911–917 (1992)
31. Wloka, J.: Partial differential equations, Cambridge University Press, Cambridge (1987)